ACS APPLIED MATERIALS & INTERFACES

Research Article

www.acsami.org

Novel Microstructural Strategies To Enhance the Electrochemical Performance of $La_{0.8}Sr_{0.2}MnO_{3-\delta}$ Cathodes

L. dos Santos-Gómez,[†] E. R. Losilla,[†] F. Martín,[‡] J. R. Ramos-Barrado,[‡] and D. Marrero-López*[,‡,§]

[†]Departamento de Química Inorgánica and [‡]Departamento de Física Aplicada I e Ingeniería Química, Laboratorio de Materiales y Superficie, Universidad de Málaga, 29071 Málaga, Spain

Supporting Information

ABSTRACT: Novel strategies based on spray-pyrolysis deposition are proposed to increase the triple-phase boundary (TPB) of $La_{0.8}Sr_{0.2}MnO_{3-\delta}$ (LSM) cathodes in contact with yttria-stabilized zirconia (YSZ) electrolyte: (i) nanocrystalline LSM films deposited on as-prepared YSZ surface; (ii) the addition of poly(methyl methacrylate) microspheres as pore formers to further increase the porosity of the film cathodes; and (iii) the deposition of LSM by spray pyrolysis on backbones of $Zr_{0.84}Y_{0.16}O_{1.92}$ (YSZ), $Ce_{0.9}Gd_{0.1}O_{1.95}$ (CGO), and $Bi_{1.5}Y_{0.5}O_{3-\delta}$ (BYO) previously fixed onto the YSZ. This last method is an alternative to the classical infiltration process with several advantages for large-scale manufacturing of planar solid oxide fuel cells (SOFCs), including easier industrial implementation, shorter preparation time, and low cost. The morphology and electrochemical performance of the electrodes are investigated by scanning electron microscopy and impedance spectroscopy. Very low values of area specific resistance are obtained, ranging from 1.4 Ω·cm^2 for LSM films deposited on as-prepared YSZ surface to 0.06 Ω·cm^2 for LSM deposited onto BYO backbone at a measured temperature of 650 °C. These electrodes exhibit high performance even after annealing at 950 °C, making them potentially suitable for applications in SOFCs at intermediate temperatures.

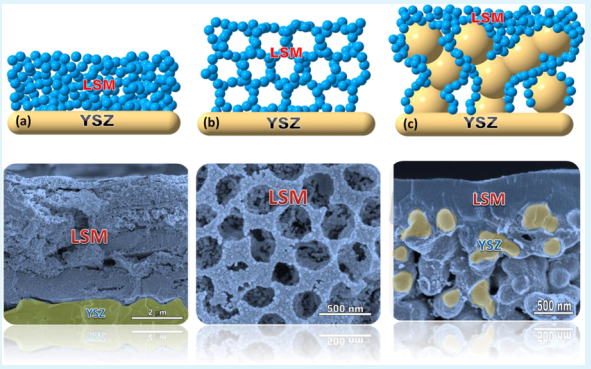

KEYWORDS: *fuel cells, $La_{0.8}Sr_{0.2}MnO_{3-\delta}$, spray pyrolysis, microstructure, impedance spectroscopy*

1. INTRODUCTION

Solid oxide fuel cells (SOFCs) are considered to be one of the most efficient technologies for direct conversion of fuels to electricity. The high operating temperature of these devices favors the oxide ion mobility and the oxygen reduction reactions at the cathode; however, this results in high costs and premature degradation of the cell components.[1,2] Consequently, lowering the operating temperature of the SOFC to the intermediate temperature range (500−700 °C) has become the main challenge for this technology.

The oxygen reduction reaction (ORR) at the cathode is responsible for much of the loss in performance at low temperature when thin film electrolytes are used.[3−5] Novel cathode materials and fabrication processes have been investigated in past few years for the development of low-temperature SOFCs. In this context, several cathode materials with high mixed ionic and electronic conductivity have been identified, e.g., $La_{0.6}Sr_{0.4}CoO_{3-\delta}$, $Ba_{0.5}Sr_{0.5}Co_{0.8}Fe_{0.2}O_{3-\delta}$, and $GdBaCo_2O_{5-\delta}$. Nevertheless, the practical applications of these cathodes are limited by the reactivity with the widely used yttria-stabilized zirconia (YSZ) electrolyte and low phase stability due to Sr/Ba segregation and carbonation at the electrode surface.[6−9] As a result, lanthanum strontium manganites (LSM) are still the preferable cathode material for commercial use.[1,2]

However, LSM exhibits poor catalytic activity for oxygen reduction at reduced temperature because of its low ionic conductivity, thus limiting the triple-phase boundary (TPB) sites at the electrolyte−electrode interface. It is generally assumed that the TPB of SOFC electrodes, at which gas, electrode, and electrolyte phases are simultaneously in contact, serve as the predominant site for the electrochemical reactions.[3] In this sense, various fabrication techniques have been investigated to obtain increased TPB lengths: (i) nanostructures LSM cathodes, including nanoparticles, nanofibers, and thin films;[10−16] (ii) polymer templating methods to increase the porosity of the electrodes;[17−19] (iii) the infiltration of LSM into electrolyte backbones;[20−22] and (iv) composites of LSM with highly conductive materials, such as $Bi_2O_{3-\delta}$.[23−26]

The preparation of electrodes via infiltration of a cation solution into a porous electrolyte backbone is one of the most effective methods used to increase the TPB area and to improve the cathode efficiency at lower temperature, especially in laboratory-scale research. However, this procedure usually requires multiple impregnation−calcination processes, complicating its implementation at industrial scale.[27,28] Thus, new and

Received: January 9, 2015
Accepted: March 20, 2015
Published: March 20, 2015

DOI: 10.1021/acsami.5b00255
ACS Appl. Mater. Interfaces 2015, 7, 7197−7205

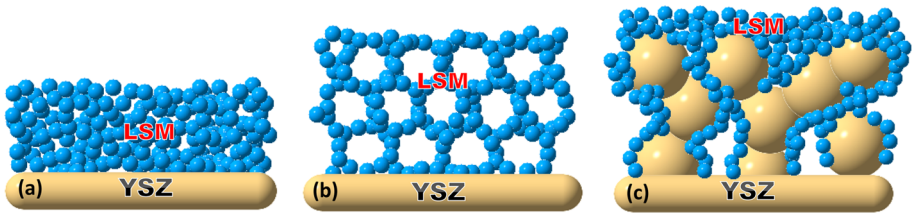

Figure 1. Schematic of the different cathodes deposited by spray pyrolysis on as-prepared electrolyte surface (a) without and (b) with PMMA as pore former and (c) electrolyte backbone.

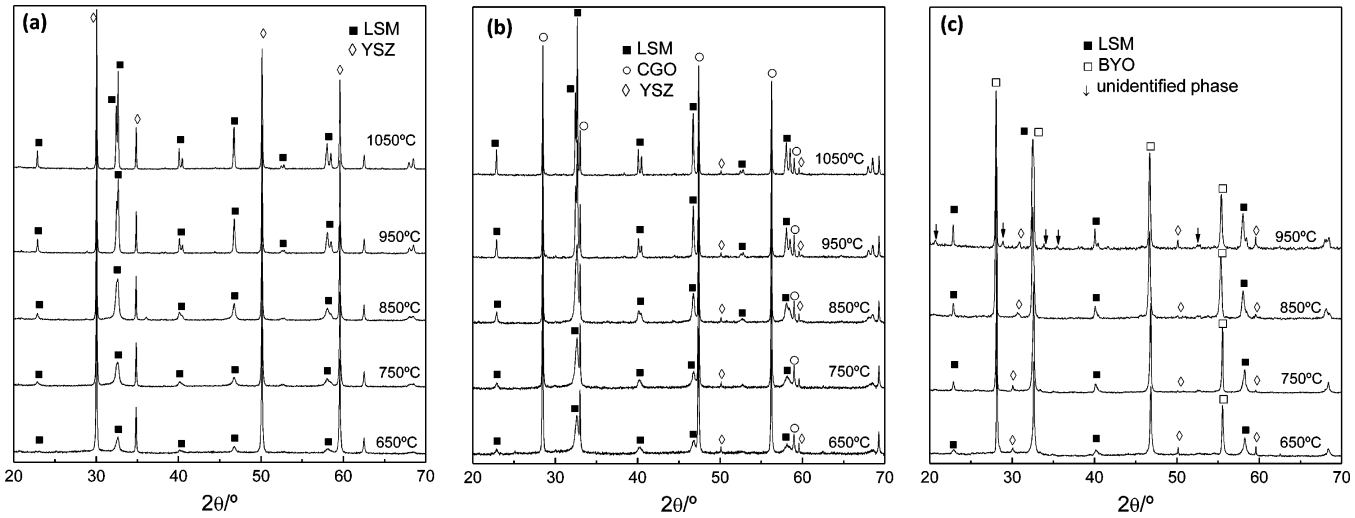

Figure 2. Selected region of XRD patterns for LSM deposited by spray pyrolysis on (a) YSZ, (b) CGO, and (c) BYO backbones after annealing between 650 and 1050 °C for 4 h. Extra diffraction peaks associated with unidentified reaction products are observed in (c).

simple methods for electrode preparation at low temperature in only one step are required.

In a previous work, LSM cathodes were deposited in a single step by spray pyrolysis onto YSZ electrolytes, obtaining polarization resistance values of 0.13 Ω·cm^2 at 750 °C (Figure 1a).[29]

In this study, alternative procedures based on spray-pyrolysis deposition have been investigated. The first is the addition of poly(methyl methacrylate) (PMMA) microspheres in the precursor solution as sacrificial template to further increase the porosity of LSM (Figure 1b). Second, the deposition of LSM by spray pyrolysis on backbones of $Zr_{0.84}Y_{0.16}O_{1.92}$ (YSZ), $Ce_{0.9}Gd_{0.1}O_{1.95}$ (CGO), and $Bi_{1.5}Y_{0.5}O_3$ (BYO) electrolytes (Figure 1c). The structure, microstructure, and electrochemical performance of these electrodes are evaluated comparatively in this work.

2. EXPERIMENTAL SECTION

2.1. Sample Preparation. The YSZ substrates were prepared from commercial powders (Tosoh) by pressing them into disks of 10−30 mm of diameter and 1 mm of thickness at 75 MPa and then sintered at 1400 °C for 4 h, reaching a relative density higher than 95%.

Porous backbones of $Zr_{0.84}Y_{0.16}O_{1.84}$ (YSZ), $Ce_{0.9}Gd_{0.1}O_{1.95}$ (CGO), and $Bi_{1.5}Y_{0.5}O_3$ (BYO) were formed by screen-printing a mixture of these powders with Decoflux (WB41, Zschimmer and Schwarz) 50:50 wt % on both sides of the YSZ pellets and then sintered at 1200 °C for 1 h for YSZ and CGO, and 850 °C for BYO. The CGO powders were supplied by Rhodia and BYO powders were prepared by a freeze-drying precursor method, following a procedure similar to that previously described for related materials.[30]

The precursor solution of $La_{0.8}Sr_{0.2}MnO_{3-\delta}$ (LSM) for spray pyrolysis was prepared by dissolving stoichiometric quantities of $La(NO_3)_3{\cdot}6H_2O$ (99.99%), $Sr(NO_3)_2$ (99.9%), and $Mn(NO_3)_2{\cdot}6H_2O$ (99%) (Sigma-Aldrich) in distilled water with a concentration of 0.025 M.

The cathodes with PMMA as pore former were obtained by adding 1.5 g of PMMA microspheres, with a diameter of 400 nm, into 50 mL of the precursor solution. Note that the small size and low density of PMMA (1.16 g/cm^3) help keep the microspheres in suspension, ensuring the same concentration during the spray deposition.

The precursor solutions were sprayed onto both faces of the YSZ pellets by using homemade spray-pyrolysis equipment. The substrates were heated at 200 °C on an aluminum block with resistance wires and the temperature was monitored with a K-type thermocouple positioned close to the sample. The substrates were continuously moved at a controlled speed underneath the spray nozzle to ensure a more homogeneous deposition of the catalyst. A stream of compressed air gas through the nozzle was used for the atomization of the solution into very fine droplets at a pressure of 2 bar. The nozzle-to-substrate distance and flow rate of the precursor solution were 20 cm and 20 mL/h, respectively. The deposition time was 1 h on each face of the substrates.

During the deposition process at 200 °C the nitrates melt and incorporate into the porous backbone. This low temperature also ensures that the PMMA microspheres do not degrade during the spray deposition, acting as pore formers. After the deposition, the cells were calcined in air at 650 °C for 4 h to reach crystallization and remove the polymer template. All electrodes showed good adhesion to the electrolyte after the deposition and successive thermal treatment up to 1050 °C.

2.2. Sample Characterization. The samples were structurally analyzed by X-ray powder diffraction (XRD) by using a PANalytical X'Pert Pro diffractometer with Cu$K\alpha_1$ radiation. The scans were collected in the 2θ range (20−80°) with a 0.016° step for 1 h. The

DOI: 10.1021/acsami.5b00255
ACS Appl. Mater. Interfaces 2015, 7, 7197−7205

phase identification and analysis were performed using the X'Pert HighScore Plus and FullProf software.[31,32]

The morphology of the electrodes was examined by field emission SEM (Helios Nanolab 650, FEI) combined with energy-dispersive spectroscopy (EDS).

The symmetrical cells were analyzed by impedance spectroscopy in air with a Solartron 1260 FRA in the $0.01-10^6$ Hz frequency range with an ac voltage of 50 mV. Pt meshes were used as current collectors.

The cells were annealed between 750 and 950 °C for 4 h in air and the impedance spectra were acquired after each postannealing treatment on the cooling process in steps of 50 °C with a dwell time of 15 min between consecutive measurements. The impedance spectra were also collected as a function of the oxygen partial pressure (pO_2) from 1 to 10^{-3} atm with an electrochemical cell equipped with a YSZ oxygen pump and sensor. The data were fitted with equivalent circuits using the ZView software to study separately the different electrode contributions involved in the ORR.[33]

3. RESULTS AND DISCUSSION

3.1. Phase Formation and Structure. Figure 2 shows the XRD patterns of LSM electrodes deposited by spray pyrolysis onto the different electrolytes backbones. Two main crystalline phases are observed, corresponding to the LSM electrode with perovskite structure and the electrolyte backbone with fluorite-type structure. Low-intensity diffraction peaks attributed to the YSZ substrate are also identified in Figure 2b,c at $2\theta = 30°$ and 50°. The as-deposited electrodes at 200 °C are amorphous and they crystallize into a single phase with rhombohedral structure ($R\bar{3}c$ space group) at 650 °C. A similar behavior is observed for LSM films deposited on YSZ electrolyte without and with PMMA microspheres.

The crystallinity of LSM enhances with increasing temperature and extra diffraction peaks ascribed to secondary phases are not observed for cells with YSZ and CGO backbones up to 1050 °C. However, additional diffraction peaks are observed for LSM deposited on BYO after annealing at 950 °C, associated possibly with the formation of unidentified reaction products and also Bi_2O_3 evaporation due to the low melting temperature of this compound.

One of the basic requirements for a composite cathode is that both cathode and backbone should be immiscible to prevent the formation of undesirable phases and the consequent loss of performance. It has been reported that LSM may react with YSZ to form insulating phases, e.g., $SrZrO_3$ and $La_2Zr_2O_7$.[34] Such phases are not identified up to 1050 °C, indicating that no appreciable reaction takes place between LSM and YSZ in the temperature range studied.

Figure 3 displays the evolution of the unit cell volume for the different phases and crystallite size of LSM with the annealing temperature. The unit cell volume of YSZ and CGO backbone remains practically unaffected by the annealing temperature, further confirming a negligible reactivity with LSM up to at least 1050 °C (Figure 3a). However, the cell volume of BYO increases slightly above 850 °C, which seems to indicate certain reactivity between the materials, possibly related to cation interdiffusion between LSM and BYO. The unit cell volume of LSM increases with the temperature from 349.96(2) Å^3 at 650 °C to 351.30(1) Å^3 at 1050 °C, which may be explained by differences in crystallite size and oxygen content in the lattice as the temperature increases (Figure 3b). These unit cell volumes are in good agreement with those previously reported for similar compositions.[35] In the case of LSM deposited onto BYO a further increase of the cell volume is observed at 950 °C,

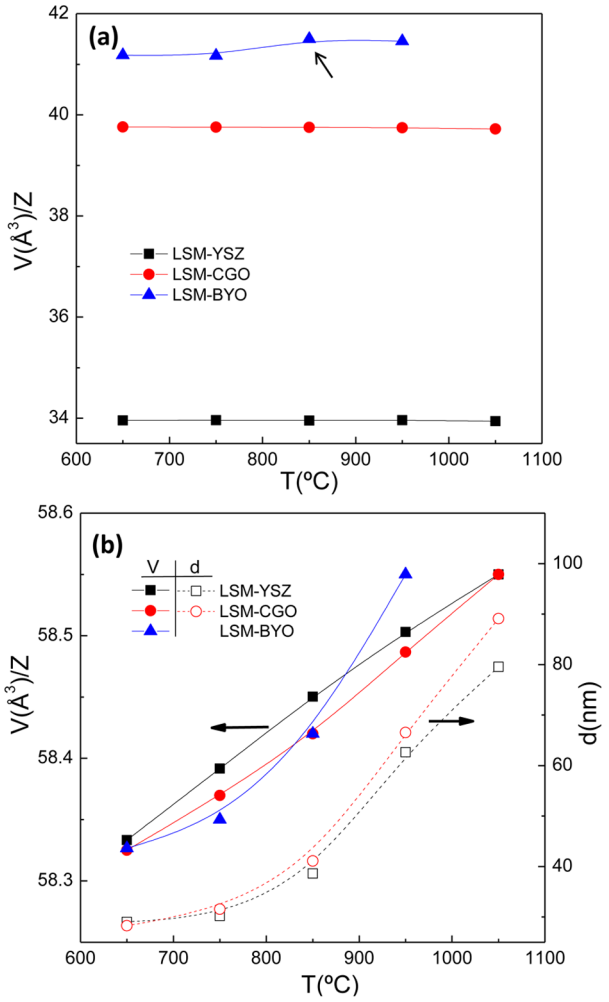

Figure 3. (a) Variation of the unit cell volume for the electrolyte backbones and (b) variation of the unit cell volume (closed symbols) and crystallite size d (open symbols) for LSM as a function of the annealing temperature.

confirming the reactivity between both materials at this temperature. Thus, the combined used of LSM and BYO is limited below 850 °C.

The average crystallite size of LSM, estimated by Scherrer's equation, increases by a factor of 3 with the annealing temperature from 28 to 90 nm in the range of 650–1050 °C (Figure 3b).

3.2. Microstructure. A cross-sectional image of the LSM cathode deposited on an as-prepared YSZ surface is shown in Figure 4. The cathode exhibits good adhesion to the substrate without appreciable delaminations or cracks. A porous microstructure is observed, which extends throughout the whole thickness ~5 μm, ensuring effective gas diffusion (Figure 4b). This high porosity is a consequence of the low deposition temperature and the remaining solvent after the deposition, which is eliminated in the subsequent thermal treatment. The grain size is lower than 50 nm at 750 °C and grows up to 190 nm after annealing at 950 °C.[29]

The cathodes prepared with PMMA microspheres are cracked as a consequence of the excessive shrinkage of the films during the decomposition of the PMMA. As can be observed, the porosity of the electrode is greatly improved with the addition of PMMA microspheres, exhibiting a homoge-

DOI: 10.1021/acsami.5b00255
ACS Appl. Mater. Interfaces 2015, 7, 7197–7205

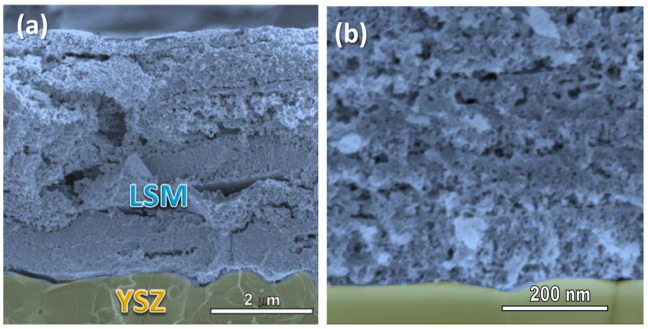

Figure 4. SEM images of the cross section of LSM cathodes deposited on as-prepared YSZ surface after annealing at 750 °C at (a) low and (b) high magnification.

neous pore arrangement (Figure 5a). The average pore size, estimated from the SEM images, is around 300 nm, which

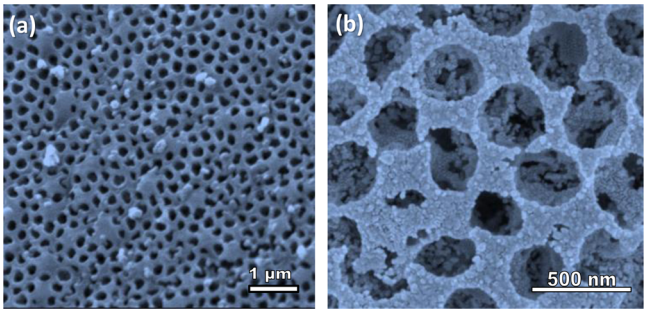

Figure 5. SEM at different magnification of the LSM surface cathode prepared with PMMA as pore formers at (a) low and (b) high magnification.

corresponds to 25% shrinkage with respect to the initial microsphere diameter (Figure 5b). It should be noted that a reduction in the concentration of PMMA microspheres would avoid an excessive shrinkage of the films, minimizing the formation of cracks.

LSM electrodes were prepared by spray pyrolysis on YSZ backbones for different deposition times, between 15 min and 1 h (Figure S1, Supporting Information). Discrete particles of LSM are formed on the surface of YSZ backbone for low deposition times ($t \leq 15$ min). For longer times, a continuous LSM coating is obtained. The microstructure of the LSM electrodes deposited by spray pyrolysis for 1 h on YSZ backbone is shown in Figure 6. The YSZ skeleton has a thickness of 10 μm and a continuous LSM coating is formed throughout the entire electrolyte backbone after spray-pyrolysis deposition (Figure 6a). SEM images at higher magnification reveal that the LSM coating has a strong bonding with YSZ surface and average thickness of 50 nm (Figure 6c). The most remarkable feature of this novel preparation method, compared to the conventional impregnation, is the formation of a thick LSM film of 500 nm on the electrode surface. This superficial film is porous as can be observed in Figure 6d, providing a current collector layer that enhances the electrical conductivity of the electrode, and possibly its electrochemical performance.

The microstructure of LSM deposited on CGO and BYO backbones is displayed in Figure S2 (Supporting Information). LSM−CGO shows similar morphology to that of LSM−YSZ. In contrast, LSM−BYO presents lower porosity and large BYO grains due to the low sintering temperature of this electrolyte in

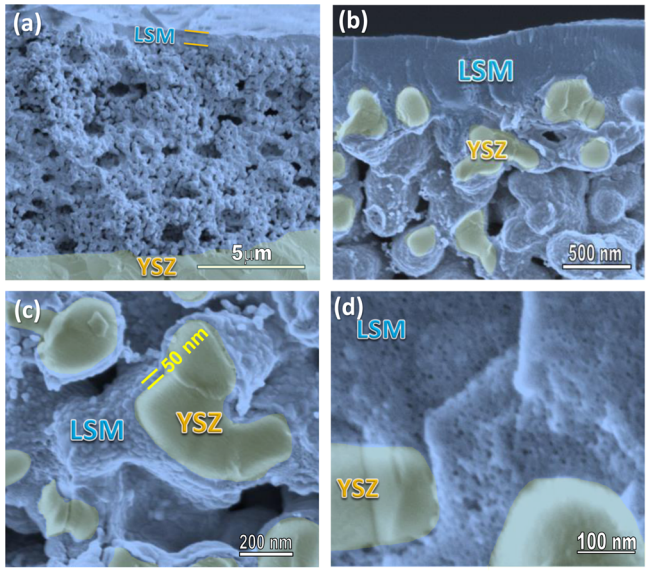

Figure 6. SEM images of the cross section of LSM cathodes deposited by spray pyrolysis on YSZ backbone, showing a YSZ backbone of 10 μm of thickness (a) with well-adhered LSM coating on the YSZ surface (b and c). A porous and superficial LSM film of 500 nm of thickness is formed (d), which acts as a current collector layer.

comparison to YSZ and CGO. In both electrodes LSM forms a continuous coating on the entire backbone thickness, ensuring a high TPB length and effective current collection.

The quantity of the deposited LSM was determined by weighing the samples before and after the spray-pyrolysis deposition, resulting in a weight ratio LSM:YSZ of 0.25:1. It is worth noting that to obtain the same content of electrode by the classical infiltration method multiple impregnation−calcination steps were necessary.[36,37]

The reason for the easy penetration of the precursor solution in the entire electrolyte skeleton is attributed to different factors: its low thickness (~10 μm); the low concentration of the precursor solution (0.025 M) compared to the classical infiltration method (0.25−1 M);[28] the low solution flow rate and the heating of the substrate, which reduces the solution viscosity and improves its penetration into the backbone. Moreover, organic additives are not used, reducing the calcination temperature and enhancing the adherence of the coating with the surface of YSZ grains. Note that in most of the wet infiltration methods, complexing agents, such as citric acid, are necessary to prevent phase segregations. In this alternative method, pure LSM are obtained without the addition of organic additives, contrary to previous works, where the direct decomposition of an aqueous solution of nitrates did not yield a pure LSM phase.[21]

Several improvements could be made by optimizing the properties of the backbone, such as porosity and tortuosity. For instance, single-graded porous electrode scaffold prepared by freeze-tape casting would facilitate the penetration of the precursor solution.[38] The deposition conditions of the spray-pyrolysis equipment could also be changed; i.e., lower deposition temperatures would allow the penetration of the solution in thicker backbones and the temperature could be varied during the deposition process to decompose in situ the precursors without the need for heating in an external furnace. Moreover, the electrodes can be deposited through a mask in an appropriate shape on the electrolyte surface to avoid a

DOI: 10.1021/acsami.5b00255
ACS Appl. Mater. Interfaces 2015, 7, 7197−7205

possible mixture of elements between the cathode and anode, which is not ruled out when wet infiltration is used. Hence, the optimization of this novel method would be an alternative to the classical infiltration with several advantages for the industry of planar SOFCs, allowing the deposition of a wide variety of electrodes over large areas with more uniform distribution of the catalyst in only one deposition step, higher reproducibility, and lower costs.

The morphology of the electrodes after annealing at 950 °C is shown in Figure S3 (Supporting Information). The grain size grows to 100 nm and the superficial porosity decreases substantially. On the other hand, the LSM coating is still continuous in the entire electrode thickness to achieve adequate current collection. Nevertheless, the grain growth reduces the TPB area, and consequently, the electrocatalytic activity for oxygen reduction decreases at high annealing temperatures as studied below.

3.3. Electrochemical Characterization. Impedance spectra for the different symmetrical cells, measured at open circuit voltage, are displayed in Figure 7. For direct comparison of the electrode response, the electrolyte resistance was subtracted. In the high-temperature range (T > 600 °C) only overlapping arcs ascribed to the electrode processes are observed (Figure 7a). Below 500 °C four different contributions are discernible, corresponding to the grain interior (GI) and grain boundary (GB) conduction through the electrolyte and two additional processes of the electrode polarization at low frequency (Figure 7b).

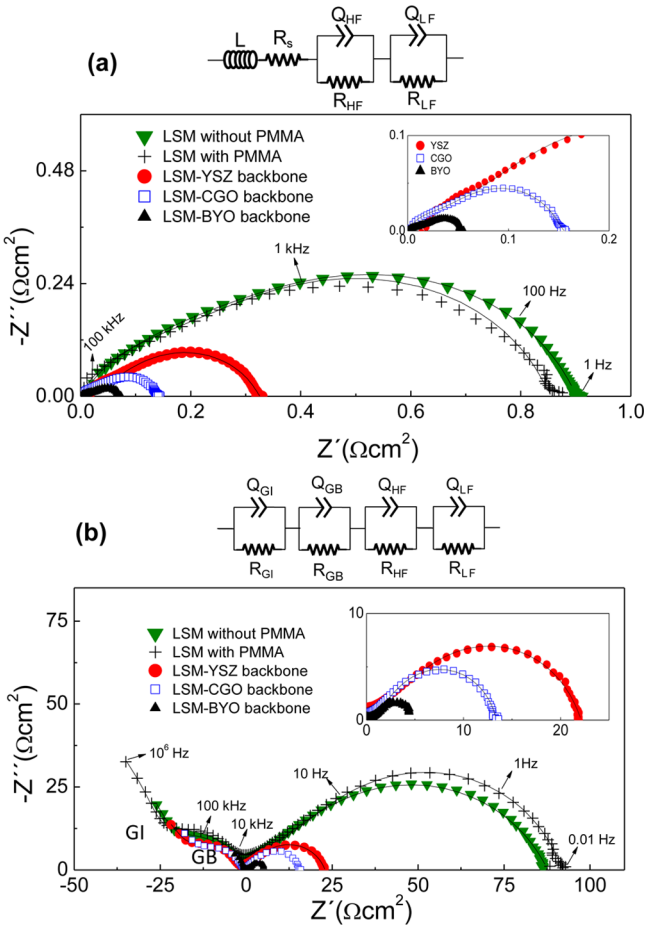

Figure 7. Impedance spectra for the different LSM cathodes after annealing at 750 °C for 4 h and measured at (a) 650 and (b) 450 °C in air at open circuit voltage. The line plots correspond to the fitting results obtained with the equivalent circuits.

The impedance spectra were analyzed by equivalent circuits composed of (RQ) elements in series, each one being assigned to a specific electrochemical phenomenon, where R is a resistance in parallel with a constant phase element Q. The electrode response of LSM is typically composed of two or three contributions depending on the electrode composition, microstructure, and measured temperature.[39,40] In the present study, the electrode response shows similar shapes for all the cells, indicating the presence of similar processes, which are adequately fitted by using two serial (RQ) elements. A serial inductance L and resistance R_s are included to simulate the inductive effects of the equipment and the electrolyte resistance respectively at high temperature (Figure 7a). Additional (RQ) elements are used to fit the GI and GB contributions of the YSZ electrolyte at low temperature (Figure 7b).

The GI and GB contributions of the YSZ show typical capacitance values of 4 pF·cm^{-1} and 8 nF·cm^{-1}, respectively, whereas the capacitance of the electrode is much larger: ∼0.1 and 1 mF·cm^{-2} for the high-frequency (HF) and low-frequency (LF) processes, respectively.

The electrolyte resistance (grain interior + grain boundary) does not depend on the preparation method, confirming negligible reactivity between the electrodes and electrolyte at the different annealing temperatures studied, in good agreement with the XRD results. However, the polarization resistance is strongly affected by the preparation method. LSM obtained on as-prepared YSZ surface with and without PMMA microspheres exhibit comparable polarization resistance values. In contrast, a substantial improvement is observed for LSM electrodes deposited onto the electrolytes backbones due to increased TPB sites (insets Figure 7). The lowest values of polarization resistance are found for BYO backbone and attributed to the higher ionic conductivity and surface exchange coefficient k_s of BYO compared to YSZ and CGO.[26,42]

To identify the different rate-limiting steps involved in the oxygen reduction reactions, the impedance spectra were acquired as a function of pO_2. The spectra for LSM deposited on YSZ backbone show two different contributions at LF and HF, being the low-frequency step is dominant at reducing pO_2 (Figure 8a). Similar curves were obtained for LSM deposited on CGO backbone.

The oxygen reduction on the cathode involves several oxygen partial pressure dependent processes, and the relationship between the resistance for each step and the oxygen partial pressure can be expressed as[40,41]

$$R_i = R_i^{o}(pO_2)^{-m} \quad (1)$$

where R_i^{o} is a constant and the exponent m provides information about the type of species involved in the ORR. In general, m = 1 is associated with molecular oxygen adsorption on the surface of the electrode or oxygen diffusion in the gas phase, m = 0.5 with oxygen dissociation and m = 0.25 with surface diffusion and/or charge-transfer reaction on the electrode.

The pO_2 dependence for R_{HF} and R_{LF} contributions is displayed in (Figure 8b). As can be observed, R_{HF} and R_{LF} show similar behavior for the electrodes deposited on as-prepared YSZ surface and YSZ backbone. The HF contribution is nearly independent of the pO_2 and has a low capacitance value of C_{HF} = 0.08−0.4 mF·cm^{-2}, which implies a process related to the

DOI: 10.1021/acsami.5b00255
ACS Appl. Mater. Interfaces 2015, 7, 7197−7205

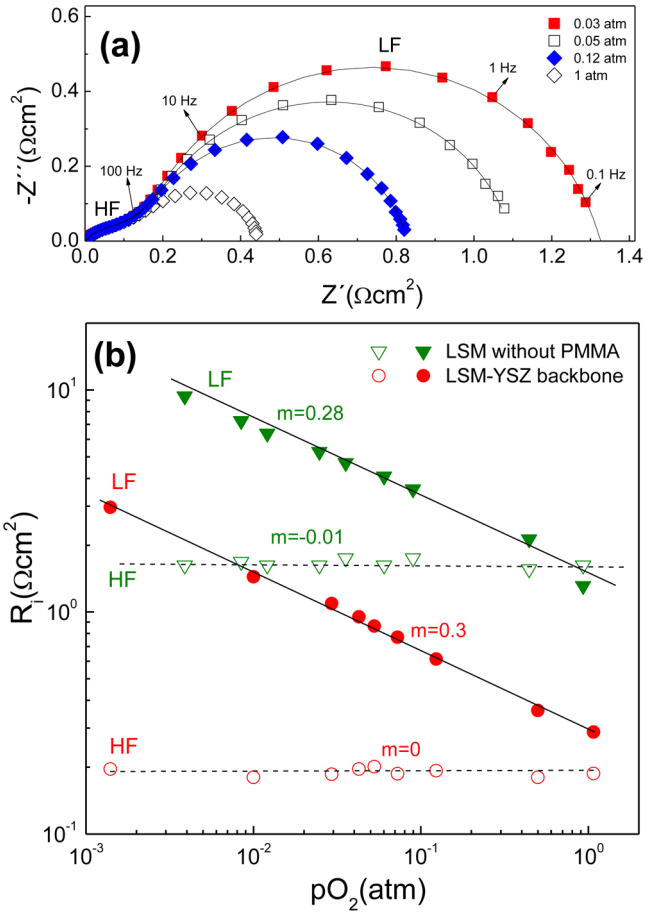

Figure 8. (a) Impedance spectra as a function of pO_2 for LSM cathodes deposited on YSZ backbone at a measured temperature of 600 °C. (b) Temperature dependence of the HF and LF resistance contributions for LSM cathode deposited on as-prepared YSZ surface and YSZ backbone.

interface, but not to the electrode surface. Consequently, the HF contribution may be assigned to oxygen ion incorporation from the TPB into the electrolyte layer or into the ionic conduction component in the composite cathodes, which is sensitive to TPB length. For LSM electrode deposited on as-prepared YSZ surface, the TPB is near the electrolyte/electrode interface. When LSM is deposited on the porous YSZ surface layer, additional TPB is formed in the bulk electrode, providing more pathways for O^{2-} incorporation and leading to lower R_H values. Additional evidence of the extended TPB in LSM deposited onto porous YSZ backbone is the increase of the electrode capacitance, which is reported to be proportional to the contact area between LSM and YSZ.[42] This increases from 0.08 mF·cm^{-2} for LSM deposited on as-prepared YSZ surface to 0.4 mF·cm^{-2} for LSM deposited on YSZ backbone.

The LF step is also sensitive to the TPB length and has an exponent m around 0.28–0.3 and capacitance of C_{LF} = 2–6.5 mF·cm^{-2} and therefore this is associated with surface diffusion and/or charge transfer ($m = {}^1/_4$).

The temperature dependence of the R_{LF} and R_{HF} contributions of the polarization in air is plotted in (Figure S4, Supporting Information). Both contributions depend on the electrode preparation and electrolyte backbone. In general, $R_{LF} > R_{HF}$ for all electrodes, indicating that oxygen incorporation at the LSM–electrolyte TPB is not the main rate-limiting step.

The activation energies for R_{HF} and R_{LF} are summarized in Table 1. The HF process shows activation energies in the range

Table 1. Area Specific Resistances at 650 °C and Activation Energies for the LSM Electrodes after Annealing at Different Temperatures[a]

sample	T (°C) annealing	ASR (Ω-cm^2)	E_{HF} (eV)	E_{LF} (eV)	E_{ASR} (eV)	reference
LSM without PMMA	750	0.91	1.13	1.32	1.22	this work
	850	1.17	1.11	1.21	1.18	
	950	3.00	1.05	1.23	1.22	
LSM with PMMA	750	0.88	1.10	1.30	1.27	this work
	850	1.30	1.14	1.22	1.25	
	950	3.40	1.08	1.25	1.23	
LSM–YSZ backbone	750	0.30	1.10	1.23	1.10	this work
	850	0.47	1.06	1.20	1.16	
	950	0.81	1.05	1.21	1.18	
LSM–CGO backbone	750	0.18	1.12	1.34	1.12	this work
	850	0.30	1.11	1.29	1.18	
	950	0.46	1.12	1.30	1.19	
LSM–BYO backbone	750	0.06	0.91	1.25	1.22	this work
	850	0.11	0.95	1.20	1.27	
LSM–YSZ	900	1.2			1.39	20
	1100	8			1.40	
LSM–30 wt % $Bi_{1.4}Er_{0.6}O_{3-\delta}$	800	0.90			1.30	23
23 wt % LSM–BYO	800	0.30			1.31	21
LSM (commercial, Praxair)	1100	9.90			1.34	this work

[a]ASRs obtained by classical infiltration method and extracted from the literature are also included for comparison.

of 0.91–1.12 eV with the lowest value corresponding to the composite with BYO, which is explained by the higher oxygen incorporation rate at the LSM/BYO interface. In contrast, the LF process has somewhat higher activation energy of 1.2–1.3 eV. These values are comparable to those reported previously for LSM composite electrodes.[26,29,42]

The area specific resistance (ASR) under open circuit voltage was calculated from the addition of each polarization contribution R_{HF} and R_{LF} and divided by 2 due to the symmetrical configuration. Figure 9 compares the temperature dependence of ASR for the different electrodes after annealing at 750 °C for 4 h. The data for a commercial LSM sample deposited by screen-printing at a sintering temperature of 1100 °C is also included for comparison. LSM films deposited on as-prepared YSZ surface show ASR values 1 order of magnitude lower than those of conventional LSM sample (e.g., 0.9 Ω·cm^2 for LSM deposited by spray pyrolysis and 9.5 Ω·cm^2 for conventional LSM at 650 °C). High porous LSM cathodes prepared with PMMA microsphere show ASR values similar to those without pore formers. This is possibly explained by the fact that large pore formers increase the porosity but do not

DOI: 10.1021/acsami.5b00255
ACS Appl. Mater. Interfaces 2015, 7, 7197–7205

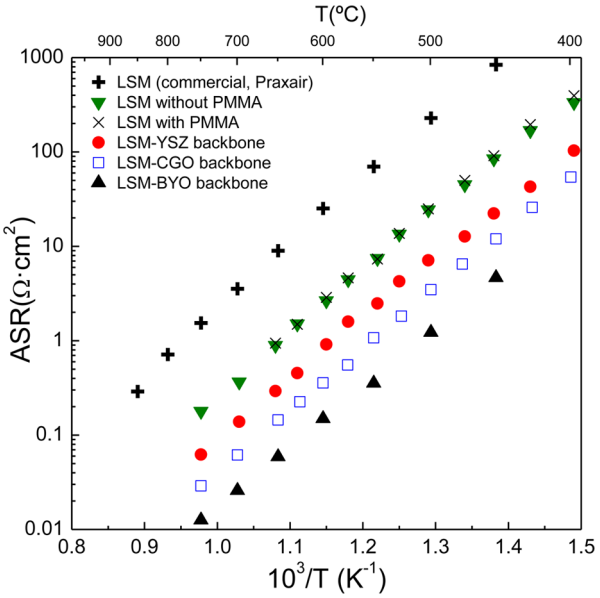

Figure 9. Temperature dependence of the area specific resistance for the different LSM cathodes annealed at 750 °C for 4 h. The data obtained with a commercial LSM cathode (Praxair) is also included for comparison.

improve significantly the surface area and TPB sites with respect to LSM without PMMA. Moreover, the presence of cracks in these electrodes reduces the current collection, negatively affecting the performance.

Electrodes deposited onto the electrolyte backbones show lower ASR due to extended TPB sites for oxygen reduction. ASR decreases in the order LSM−YSZ > LSM−CGO > LSM−BYO in good agreement with the highest ionic conductivity of Bi_2O_3-based electrolytes and the consequent fast oxygen incorporation in the lattice.

ASRs are extremely low, e.g., 0.30, 0.14, and 0.06 Ω·cm^2 for LSM−YSZ, LSM−CGO, and LSM−BYO composite cathodes at 650 °C respectively, compared to those previously reported in the literature for LSM−electrolyte composite powder mixtures: 4.9, 2.5, and 0.3 Ω·cm^2 for LSM−50 wt % YSZ, LSM−50 wt % CGO, and LSM−80 wt % BYO, respectively.[42,43] Table 1 compares the ASR values obtained in this work with those previously reported in the literature from the conventional infiltration method. As can be observed, ASRs are 5 times lower than those previously reported by Jian et al., ∼0.3 Ω·cm for 23 wt % LSM−BYO.[21] ASRs are even comparable to those obtained for nanocrystalline cobaltite cathodes with high mixed ionic−electronic conductivity, e.g., 0.04 Ω·cm^2 for $La_{0.6}Sr_{0.4}Co_{0.8}Fe_{0.2}O_{3-\delta}$.[44,45]

Another important issue to be considered is the stability of the nanostructured electrodes at high annealing temperatures due to the microstructure coarsening and the resulting decrease of TPB area and performance. Hence, it is highly relevant to evaluate the electrode response as a function of the annealing temperature. Figure S5 (Supporting Information) displays the ASR for LSM deposited on the different backbones after annealing the cells between 750 and 950 °C for 4 h. A substantial increase of the ASR is observed with increasing of annealing temperature, ranging between 0.3 and 0.83 Ω·cm^2 for LSM−YSZ cathode at a measured temperature of 650 °C (Table 1). This effect is clearly related to a reduction of the electrode−pore surface area with the consequent decreases of TPB sites for oxygen reduction.

Despite the increase of ASR with the temperature, these values are significantly lower than those reported for a conventional LSM−electrolyte composite cathode, making these electrode materials potentially suitable for intermediate temperature SOFCs.

Finally, the stability of the electrodes was evaluated for 100 h at 650 °C and both the serial and polarization resistance showed an increase of about 5%, which is related to microstructural changes of the electrodes. Further studies are in progress to evaluate the stability of these nanostructured electrodes after long-term operation and to test the performance in fuel cells.

In summary, spray deposition could be an effective method for commercial production of large-area electrodes for SOFCs with a series of advantages respect to the classical wet infiltration process, including easy industrial implementation, preparation in one single deposition/thermal step, and low cost. Moreover, this method may be applicable to other electrochemical systems, such as solid electrolyzers, batteries, and supercapacitors.

4. CONCLUSIONS

New microstructural strategies based on spray-pyrolysis deposition were investigated to improve the electrochemical properties of LSM cathodes at reduced temperatures by extending the TPB length. LSM cathodes were deposited at 200 °C on as-prepared YSZ substrates by using a precursor solution of metal nitrates in water without and with PMMA microspheres as sacrificial template. LSM electrodes with homogeneous pore size distribution were obtained with PMMA microspheres. To further increase the TPB sites, composites of LSM with different electrolytes were obtained, by spraying the solution on porous backbones of YSZ, CGO, and BYO. A continuous LSM coating is formed in the entire surface of the skeleton electrolyte.

LSM electrodes deposited on as-prepared YSZ surface with and without PMMA microspheres as pore formers exhibited similar ASR values of 0.9 Ω·cm^2 at a measured temperature of 650 °C, which is 1 order of magnitude lower than those obtained for a commercial LSM cathode prepared by screen-printing at high sintering temperatures. LSM electrodes deposited onto electrolyte backbones showed significantly lower ASR due to extended TPB sites. The lowest values were found for BYO backbone due to its higher ionic conductivity and fast oxygen incorporation into the lattice ∼0.06 Ω·cm^2 at 650 °C. The present results demonstrate that spray pyrolysis could be a versatile alternative for obtaining high-efficiency SOFC cathodes, possessing several advantages with respect to the classical wet infiltration method, such as easy industrial implementation, one single deposition step in large areas, and better reproducibility. Several modifications could be made by varying the deposition conditions and improving the porosity of the electrolyte skeleton. This study should also be extended to high mixed ionic−electronic conductors, such as $(La,Sr)(Co,Fe)O_3$ with CGO backbone, thus avoiding the use of Bi_2O_3-based electrolytes, which are reported to be unstable at intermediate temperatures.

DOI: 10.1021/acsami.5b00255
ACS Appl. Mater. Interfaces 2015, 7, 7197−7205

■ ASSOCIATED CONTENT

Supporting Information

SEM images of LSM−YSZ cathode deposited for 15 and 30 min; SEM images of LSM−CGO and LSM−BYO cathodes; SEM images of LSM−YSZ after annealing at 950 °C for 4 h; temperature dependence of the HF and LF resistance contributions of the polarization; temperature dependence of ASR as a function of annealing temperature. This material is available free of charge via the Internet at http://pubs.acs.org/.

■ AUTHOR INFORMATION

Corresponding Author

*E-mail: damarre@uma.es.

Present Address

[§]Departamento de Física Aplicada I, Laboratorio de Materiales y Superficies, Facultad de Ciencias, Campus de Teatinos, Universidad de Málaga, 29071 Málaga, Spain. Tel.: +34 952137057. Fax: +34 952132382.

Notes

The authors declare no competing financial interest.

■ ACKNOWLEDGMENTS

This work was supported by MINECO through the MAT2013-41836-R research grant (Spain) which is cofunded by FEDER. L. dos Santos-Gómez thanks the Spanish Ministry of Education, Culture and Sports for her FPU studentship.

■ REFERENCES

(1) Minh, N. Q.; Takahashi, T. *Science and Technology of Ceramic Fuel Cell*; Elsevier: New York, 1995.

(2) Vielstich, W.; Gasteiger, H. A.; Lamm, A.; Yokokawa, H. *Handbook of Fuel Cells − FundamentalsTechnology and Applications*; John Wiley & Sons: New York, 2010.

(3) Adler, S. B. Factors Governing Oxygen Reduction in Solid Oxide Fuel Cells Cathodes. *Chem. Soc. Rev.* **2004**, *104*, 4791−4843.

(4) Fleig, J. Solid Oxide Fuel Cell Cathodes: Polarization Mechanisms and Modeling of the Electrochemical Performance. *Annu. Rev. Mater. Res.* **2003**, *33*, 361−382.

(5) Tsipis, E. V.; Kharton, V. V. I Performance-Determining Factors. *J. Solid State Electrochem.* **2008**, *12*, 1039−1060.

(6) Tai, L. W.; Nasrallah, M. M.; Anderson, H. U.; Sparlin, D. M.; Sehlin, S. R. Structure and Electrical Properties of $La_{1-x}Sr_xCo_{1-y}Fe_yO_3$. Part 1. The System $La_{0.8}Sr_{0.2}Co_{1-y}Fe_yO_3$. *Solid State Ionics* **1995**, *76*, 259−271.

(7) Shao, Z.; Haile, S. M. A High Performance Cathode for the Next Generation Solid-Oxide Fuel Cells. *Nature.* **2004**, *431*, 170−173.

(8) Tarancón, A.; Skinner, S. J.; Chater, R. J.; Hernández-Ramírez, F.; Kilner, J. A. Layered Perovskites as Promising Cathodes for Intermediate Temperature Solid Oxide Fuel Cells. *J. Mater. Chem.* **2007**, *17*, 3175−3181.

(9) Švarcová, S.; Wiik, K.; Tolchard, J.; Bouwmeester, H. J. M.; Grande, T. Structural Instability of Cubic Perovskite $Ba_xSr_{1-x}Co_{1-y}Fe_yO_{3-\delta}$. *Solid State Ionics* **2008**, *178*, 1787−1791.

(10) Zhi, M.; Zhou, G.; Hong, Z.; Wang, J.; Gemmen, R.; Gerdes, K.; Manivannan, A.; Ma, D.; Wu, N. Single Crystalline $La_{0.5}Sr_{0.5}MnO_3$ Microcubes as Cathode of Solid Oxide Fuel Cell. *Energy Environ. Sci.* **2011**, *4*, 139−144.

(11) Mamak, M.; Métraux, G. S.; Petrov, S.; Coombs, N.; Ozin, G. A.; Green, M. A. Lanthanum Strontium Manganite/yttria-stabilized Zirconia Nanocomposites Derived from a Surfactant Assisted, Co-assembled Mesoporous Phase. *J. Am. Chem. Soc.* **2003**, *125*, 5161−5175.

(12) Zhi, M.; Mariani, N.; Gemmen, R.; Gerdes, K. Nanofiber Scaffold for Cathode of Solid Oxide Fuel Cell. *Energy Environ. Sci.* **2011**, *4*, 417−420.

(13) Azad, A. M. Fabrication of Yttria-stabilized Zirconia Nanofibers by Electrospinning. *Mater. Lett.* **2006**, *60*, 67−72.

(14) Sholklapper, T. Z.; Kurokawa, H.; Jacobson, C. P.; Visco, S. J.; De Jonghe, L. C. Nanostructured Solid Oxide Fuel Cell Electrodes. *Nano Lett.* **2007**, *7*, 2136−2141.

(15) Princivalle, A.; Perednis, D.; Neagu, R.; Djurado, E. Microstructural Investigations of Nanostructured $La(Sr)MnO_{3-\delta}$ Films Deposited by Electrostatic Spray Deposition. *Chem. Mater.* **2004**, *16*, 3733−3739.

(16) Im, J.; Park, I.; Shin, D. Electrochemical Properties of Nanostructured Lanthanum Strontium Manganite Cathode Fabricated by Electrostatic Spray Deposition. *Solid State Ionics* **2011**, *192*, 448−452.

(17) Ruíz-Morales, J. C.; Marrero-López, D.; Gálvez-Sánchez, M.; Canales-Vázquez, J.; Savaniu, C.; Savvin, S. N. Engineering of Materials for Solid Oxide Fuel Cells and Other Energy and Environmental Applications. *Energy Environ. Sci.* **2010**, *3*, 1670−1681.

(18) Marrero-López, D.; Ruíz-Morales, J. C.; Peña-Martínez, J.; Canales-Vázquez, J.; Núñez, P. Preparation of Thin Layer Materials with Macroporous Microstructure for SOFC Applications. *J. Solid State Chem.* **2008**, *181*, 685−692.

(19) Brown, E. C.; Wilke, S. K.; Boyd, D. A.; Goodwin, D. G.; Haile, S. M. Polymer Sphere Lithography for Solid Oxide Fuel Cells: a Route to Functional, Well-defined Electrode Structures. *J. Mater. Chem.* **2010**, *20*, 2190−2196.

(20) Chen, K.; Ai, N.; Jiang, S. P. Reasons for the High Stability of Nano-structured $(La,Sr)MnO_3$ Infiltrated Y_2O_3−ZrO_2 Composite Oxygen Electrodes of Solid Oxide Electrolysis Cells. *Electrochem. Commun.* **2012**, *19*, 119−122.

(21) Jiang, Z.; Lei, Z.; Ding, B.; Xia, C.; Zhao, F.; Chen, F. Electrochemical Characteristics of Solid Oxide Fuel Cell Cathodes Prepared by Infiltrating $(La,Sr)MnO_3$ Nanoparticles into Yttria-stabilized Bismuth Oxide Backbones. *Int. J. Hydrogen Energy* **2010**, *35*, 8322−8330.

(22) Huang, Y.; Vohs, J. M.; Gorte, R. J. SOFC Cathodes Prepared by Infiltration with Various LSM Precursors. *Electrochem. Solid-State Lett.* **2006**, *9*, A237−A240.

(23) Li, J.; Wang, S.; Wang, Z.; Liu, R.; Wen, T.; Wen, Z. $La_{0.84}Sr_{0.16}MnO_3$ Cathodes Impregnated with $Bi_{1.4}Er_{0.6}O_3$ for Intermediate-temperature Solid Oxide Fuel Cells. *J. Power Sources* **2009**, *194*, 625−630.

(24) Li, J.; Wang, S.; Wang, Z.; Liu, R.; Wen, T.; Wen, Z. $(La_{0.74}Bi_{0.10}Sr_{0.16})MnO_{3-\delta}$−$(Bi_2O_3)_{0.7}(Er_2O_3)_{0.3}$ Composite Cathodes for Intermediate Temperature Solid Oxide Fuel Cells. *J. Power Sources* **2008**, *179*, 474−480.

(25) Jiang, Z.; Xia, C.; Zhao, F.; Chen, F. $La_{0.85}Sr_{0.15}MnO_{3-\delta}$ Infiltrated $Y_{0.5}Bi_{1.5}O_3$ Cathodes for Intermediate-Temperature Solid Oxide Fuel Cells. *Electrochem. Solid State Lett.* **2009**, *12*, B91−B93.

(26) Lee, K. T.; Jung, D. W.; Yoon, H. S.; Lidie, A. A.; Camaratta, M. A.; Wachsman, E. D. Interfacial Modification of $La_{0.80}Sr_{0.20}MnO_{3-\delta}$−$Er_{0.4}Bi_{0.6}O_3$ Cathodes for High Performance Lower Temperature Solid Oxide Fuel Cells. *J. Power Sources* **2012**, *220*, 324−330.

(27) Huang, Y.; Vohs, J. M.; Gorte, R. J. Fabrication of SOFC Electrodes by Impregnation Methods. In *Advances in Electronic and Electrochemical Ceramics*; John Wiley & Sons, Inc.: Hoboken, NJ, 2006; Vol. *179*.

(28) Ding, D.; Li, X.; Lai, S.; Gerdes, K.; Liu, M. Enhancing SOFC Cathode Performance by Surface Modification Through Infiltration. *Energy Environ. Sci.* **2014**, *7*, 552−575.

(29) Marrero-López, D.; dos Santos-Gómez, L.; Canales-Vázquez, J.; Martín, F.; Ramos-Barrado, J. R. Stability and Performance of Nanostructured $La_{0.8}Sr_{0.2}MnO_3$ Cathodes Deposited by Spray-pyrolysis. *Electrochim. Acta* **2014**, *134*, 159−166.

(30) Amsif, M.; Marrero-López, D.; Magrasó, A.; Peña-Martínez, J.; Ruíz-Morales, J. C.; Núñez, P. Synthesis and Characterisation of $BaCeO_3$-based Proton Conductors Obtained from Freeze-dried Precursors. *J. Eur. Ceram. Soc.* **2009**, *29*, 131−138.

DOI: 10.1021/acsami.5b00255
ACS Appl. Mater. Interfaces 2015, 7, 7197−7205

(31) Rodríguez-Carvajal, J. Recent Advances in Magnetic Structure Determination by Neutron Powder Diffraction. *Physica B* **1993**, *192*, 55−69.
(32) X'Pert HighScore Plus, version 3.0e. PANalytical B.V.: Almelo, The Netherlands, 2012.
(33) Johnson, D. ZView: a Software Program for IES Analysis, Version 2.9. Scribner Associates, Inc.: Southern Pines, NC, 2005.
(34) Choi, J. H.; Jang, J. H.; Oh, S. M. Microstructure and Cathodic Performance of $La_{0.9}Sr_{0.1}MnO_3$/Yttria-Stabilized Zirconia Composite. *Electrochim. Acta* **2001**, *46*, 867−874.
(35) Dhahri, J.; Zemni, S.; Cherif, K.; Dhahri, J.; Oumezzine, M.; Ghedira, M.; Vincent, H. The Effect of Deficit of Strontium on Structural, Magnetic and Electrical Properties of $La_{0.8}Sr_{0.2-x}\square_xMnO_3$ Manganites. *J. Alloys Compd.* **2005**, *394*, 51−57.
(36) Bidrawn, F.; Vohs, J. M.; Gorte, R. J. Fabrication of LSM−YSZ Composite Electrodes by Electrodeposition. *J. Electrochem. Soc.* **2010**, *157*, B1629−B1633.
(37) Ni, C. S.; Vohs, J. M.; Gorte, R. J.; Irvine, J. T. S. Fabrication and Characterisation of a Large-Area Solid Oxide Fuel Cell Based on Dual Tape Cast YSZ Electrode Skeleton Supported YSZ Electrolytes with Vanadate and Ferrite Perovskite-Impregnated Anodes and Cathodes. *J. Mater. Chem. A* **2014**, *2*, 19150−19155.
(38) Cable, T. L.; Sofie, S. W. A Symmetrical, Planar SOFC Design for NASA's High Specific Power Density Requirements. *J. Power Sources* **2007**, *174*, 221−227.
(39) Siebert, E.; Hammouche, A.; Kleitz, M. Impedance Spectroscopy Analysis of $La_{1-x}Sr_xMnO_3$ Yttria-Stabilized Zirconia Electrode Kinetics. *Electrochim. Acta* **1995**, *11*, 1741−1753.
(40) Østergård, M. J. L.; Mogensen, M. Ac Impedance Study of the Oxygen Reduction Mechanism on $La_{1-x}Sr_xMnO_3$ in Solid Oxide Fuel Cells. *Electrochim. Acta* **1993**, *38*, 2015−2020.
(41) Grimaud, A.; Mauvy, F.; Bassat, J. M.; Fourcade, S.; Marrony, M.; Grenier, J. C. Hydration and Transport Properties of the $Pr_{2x}Sr_xNiO_{4+\delta}$ Compounds as H+-SOFC Cathodes. *J. Mater. Chem.* **2012**, *22*, 16017−16025.
(42) Wu, L.; Jiang, Z.; Wang, S.; Xia, C. $(La,Sr)MnO_3$−$(Y,Bi)_2O_3$ Composite Cathodes for Intermediate-Temperature Solid Oxide Fuel Cells. *Int. J. Hydrogen Energy* **2013**, *38*, 2398−2406.
(43) Murray, E. P.; Barnett, S. A. $(La,Sr)MnO_3$−$(Ce,Gd)O_{2-x}$ Composite Cathodes for Solid Oxide Fuel Cells. *Solid State Ionics* **2001**, *143*, 265−273.
(44) Chanquía, M. C.; Mogni, L.; Troiani, H. E.; Caneiro, A. Highly Active $La_{0.4}Sr_{0.6}Co_{0.8}Fe_{0.2}O_{3-\delta}$ Nanocatalyst for Oxygen Reduction in Intermediate Temperature-solid Oxide Fuel Cells. *J. Power Sources* **2014**, *270*, 457−467.
(45) Marrero-López, D.; Romero, R.; Martín, F.; Ramos-Barrado, J. R. Effect of the Deposition Temperature on the Electrochemical Properties of $La_{0.6}Sr_{0.4}Co_{0.8}Fe_{0.2}O_{3-\delta}$ Cathode Prepared by Conventional Spray-Pyrolysis. *J. Power Sources* **2014**, *255*, 308−317.

DOI: 10.1021/acsami.5b00255
ACS Appl. Mater. Interfaces 2015, 7, 7197−7205